Porphyromonas gingivalis Sphingolipid Synthesis Limits the Host Inflammatory Response

P. gingivalis sphingolipid synthesis limits the host inflammatory response

Fernanda G. Rocha[1†], Zachary D. Moye[1†], Gregory Ottenberg[1†], Peijun Tang[2†], Dominic J. Campopiano[2¶], Frank C. Gibson III[1¶*], and Mary E. Davey[1¶*]

Department of Oral Biology, College of Dentistry, University of Florida, Gainesville, Florida, USA[1], School of Chemistry, University of Edinburgh, Edinburgh, EH9 3FJ, UK[2]

[†] and [¶] contributed equally

Abstract word count (290); Total word count (3197); Total number of Tables and Figures (5); Number of References (38)

Key words: homeostasis, Bacteroidetes, inflammation, dihydroceramides, membrane microdomains, sigma factors

* Corresponding authors:

M.E. Davey, Department of Oral Biology, University of Florida, College of Dentistry, P.O. Box 100424, Gainesville, FL 32610.

Phone: (352) 273-8858

Email: mdavey@dental.ufl.edu

F.C. Gibson III, Department of Oral Biology, University of Florida, College of Dentistry,

P.O. Box 100424, Gainesville, FL 32610.
Phone: (352) 273-8856;
Email: fgibson@dental.ufl.edu

Abstract

Porphyromonas gingivalis, like other bacteria belonging to the phylum Bacteroidetes synthesizes sphingolipids (SLs). However, their exact roles in microbial physiology and their potential role in mediating interactions with their eukaryotic host are unclear. Our working hypothesis for this study was that synthesis of SLs (host-like lipids) affords a mechanism that allows *P. gingivalis* to persist in homeostasis with its host. In a previous study, we deleted a gene (PG1780 in strain W83), predicted to encode a serine palmitoyl transferase (SPT), the enzyme that catalyzes the first conserved step in the synthesis of SLs, and we determined that the mutant was unable to synthesize SLs. Here, we characterized the SPT enzyme encoded by PG1780, analyzed the impact SPT deletion on *P. gingivalis* gene expression (RNA-Seq analysis), and began to define the impact of SL synthesis on its interactions with host cells. Enzymatic analysis verified that the protein encoded by PG1780 is indeed an SPT. RNA-Seq analysis determined that a lack of SL synthesis results in differential expression of extracytoplasmic function (ECF) sigma factors, components of the Type IX secretion system (T9SS), and CRISPR and *cas* genes. When human THP1 macrophage-like cells were challenged with the wild-type (W83) and the SL-null mutant (W83 ΔSPT), our data demonstrate that the SL-null strain elicits a robust inflammatory response (elevated IL-1β, IL-6, IL-10, IL-8, RANTES, and TNFα) while the response to the parent strain W83 is negligible. Interestingly, we also discovered that SLs

47 produced by *P. gingivalis* can be delivered to host cells independent of cell-to-cell contact.
48 Overall, our results support our working hypothesis that synthesis of SLs by *P. gingivalis* is
49 central to its ability to manipulate the host inflammatory response and demonstrate the integral
50 importance of SLs in the physiology of *P. gingivalis*.
51
52

Introduction

Sphingolipids (SLs) are a class of amphipathic lipids containing a long-chain amino alcohol backbone (also called a sphingoid base) attached via an amide linkage to a fatty acyl chain. The first committed step in the generation of SLs is the condensation of an amino acid, often serine, and palmitoyl CoA to form sphinganine by the enzyme serine palmitoyl transferase (SPT) (Harrison et al. 2018; Merrill and Carman 2015). SLs play a prominent role in numerous eukaryotic cellular processes including inflammation, cell migration, adhesion, growth, and apoptosis (Hannun and Obeid 2008; 2018; Maceyka and Spiegel 2014; Merrill and Carman 2015); and they have been linked to a growing number of inborn genetic diseases (Dunn et al. 2019).

While SL synthesis is ubiquitous in eukaryotes, it is rare in prokaryotes. Intriguingly, a variety of bacteria belonging to the phylum Bacteroidetes that persist in the oral microbiome, including *P. gingivalis*, *Tannerella forsythia*, and *Prevotella intermedia* are proficient in SL synthesis (Olsen and Jantzen 2001). Although SLs produced by these bacteria are highly similar to the host SLs, these lipids are distinct in their head groups and an iso-methyl branch in both the long chain base and ceramide component (Harrison et al. 2018.). Practically, these chemical distinctions are highly significant since they have been used to detect and distinguish bacterially-derived SLs (Brown et al. 2019; Nichols et al. 2004). In particular, the SLs produced by oral anaerobes, including *P. gingivalis* have been shown to permeate host tissues (Nichols 1998; Nichols and Rojanasomsith 2006; Nichols et al. 2011), and the types of SLs were found to be distinct in healthy versus diseased tissues (Nichols and Rojanasomsith 2006; Nichols et al. 2011). Given that *P. gingivalis* is strongly implicated in the etiology of periodontal disease (Byrne et al. 2009; Darveau 2010; Lamont and Jenkinson 1998; Socransky et al. 1998);

76 understanding the impact of SLs on the physiology of this bacterium as well as defining their
77 impact on the host as purified lipids have been investigated (Moye et al. 2016; Olsen and Nichols
78 2018). Purified SLs derived from *P. gingivalis* induce a number of changes in the physiology of
79 eukaryotic cells *in vitro* (Olsen and Nichols 2018), and often these effects are only observed for
80 SLs bearing a particular headgroup. For example, phosphoglycerol dihydroceramide induce the
81 RANKL-dependent pathway of osteoclastogenesis in osteoclasts (Kanzaki et al. 2017), initiate
82 apoptosis in endothelial cells (Zahlten et al. 2007), and increase the generation of prostaglandin
83 E2 by gingival fibroblasts (Nichols et al. 2004). In model systems of disease,
84 phosphoethanolamine dihydroceramides induced inflammation in a murine model of
85 experimental autoimmune encephalomyelitis (Nichols et al. 2009). Thus, SLs synthesized by *P.*
86 *gingivalis* profoundly impact a variety of eukaryotic signaling pathways in a highly cell-specific
87 and lipid-specific manner and may form a link to systemic conditions.
88 While there are few reports describing the role of bacterially-derived SLs in bacterial
89 physiology or membrane structure and function, the data indicate that they may function in
90 similar ways as in eukaryotic cells (Heaver et al. 2018). Studies with *B. fragilis* have
91 demonstrated the formation of SL-dependent membrane microdomains, similar to eukaryotic
92 lipid rafts and that SLs are essential for mounting a stress response and long-term survival,
93 suggesting that SLs play a role in regulating gene expression (An et al. 2011). We recently
94 demonstrated that SLs are essential for *P. gingivalis* survival under oxidative stress. Also, we
95 determined that select SLs are present in outer membrane vesicles (OMVs) thereby identifying a
96 potential mechanism of SL-secretion (Moye et al. 2016). Here, we define the enzyme kinetics of
97 the SPT produced by *P. gingivalis* and describe a working model where SLs regulate gene
98 expression via ECF sigma factors. Further, we show a hyper inflammatory response of

macrophage-like cells when cultured with the SL null mutant. Interestingly, we also discovered that *P. gingivalis* can deliver its SLs to host cells in a contact-independent manner. Overall, our studies exemplify the integral importance of SLs in the physiology of *P. gingivalis* and provide new evidence supporting the concept that like other members of the Bacteroidetes, synthesis of SLs by *P. gingivalis* is likely central to its ability to manipulate the host inflammatory response.

Methods (see appendix for details)

Purification and characterization of SPT enzyme

The PG1780 gene (strain W83) was cloned into expression plasmids which contained either a C-terminal stop codon in lieu of a tag (PgSPT), a C-terminal ten-histidine tag (pEBSRCTEVC$_{10}$HIS), or an N-terminal six-histidine tag (pEHISTEV). Constructs were transformed into *E. coli* BL21 (DE3) competent cells. PgSPT was purified either by nickel affinity column chromatography (His-tagged) or by HiTrap anion exchange chromatography (non-tagged), followed by gel-filtration chromatography. Purification was monitored by SDS-PAGE and size characterized by LC-ESI-MS. Dissociation constants (K_d) were determined by UV-visible absorbance spectrophotometry. Kinetic experiments were performed using a 5,5'-dithiobis-2-nitrobenzoic acid (DTNB) assay and resultant products were measured using MALDI-TOF-MS.

RNA-Seq Analysis

P. gingivalis strain W83 was used in this study along with the matching SPT mutant (W83 ΔPG1780), which was generated and characterized previously (Moye et al. 2016). RNA was extracted from cells grown anaerobically in TSBHK to an O.D.$_{600}$ of 1.0, the quality was then

assessed and sequencing was performed and analyzed as previously described (Moradali et al. 2019; Moye et al. 2019).

Host cell cytokine/chemokine profiling

The human cell line THP-1 was maintained in RPMI-1640+10%FBS and differentiated for 48h into macrophage-like cells using 100nM phorbol 12-myristate 13-acetate (PMA), and $5x10^5$ cells were seeded into 24-well tissue culture plates. Parent or ΔSPT mutant *P. gingivalis* (cultured as above) were added to THP-1 cells (MOI 100) and following 2 h, 6 h and 24 h of incubation cell culture supernatant fluids were collected and cytokine and chemokine levels were determined by Milliplex Multiplex Assays using a Luminex 200® system. THP-1 cell viability was assessed by MTT assay.

***P. gingivalis* sphingolipid labeling and tracking**

SL-labeling was performed as previously described for *Bacteroides thetaiotamicron* (Johnson et al. 2019) with slight modifications. Briefly, *P. gingivalis* strains were cultured for 24hrs in rich medium and transferred into chemically defined medium (Vermilyea et al. 2019) supplemented with chemically modified palmitic acid containing an alkyne (PAA). PMA-differentiated THP-1 cells were placed in the bottom wells of 24-well plates containing sterile glass coverslips. Sterile 0.4μm pore-size transwell inserts were placed into the wells of the cell culture dishes and $1x10^9$ bacteria were then placed in the upper chamber. After 24hr of culture at 37°C + 5% CO_2, coverslips were removed, washed then Click-labeled with an azide-488 fluorophore using manufacturers specifications. Coverslips were mounted onto slides with a DAPI-containing

medium and were imaged by fluorescence microscopy. W83 parent and SPT mutant +PAA were Click-labeled directly to validate PAA incorporation and labeling only in the parent.

Results

SPT sequence comparisons

All bacterial SPTs are members of the pyridoxal-5'phosphate(PLP)-dependent α-oxoamine synthase (AOS) family, catalyzing Claisen-like condensation reactions between acyl-CoA substrates and amino acid to form different α-oxoamine products (Harrison et al. 2018). In the case of SPT, this would be ketodihydrosphingosine (KDS). The average amino acid sequence similarity across the AOS enzymes is ~30-35%, depending on different functions (see Supplemental Table 1 and Supplemental Figure 1A). The amino acid sequence alignment between *Sphingomonas paucimobilis* SPT (SpSPT, Q93UV0) (Yard et al. 2007) *Bacteroides fragilis* SPT (BfSPT, Q5LCK4) and *P. gingivalis* SPT (PgSPT, W1R7E5) shows high sequence homology, with conservation of key residues involved in PLP-binding and catalysis. Moreover, gut human microbial BfSPT shares the highest amino acid sequence identity (76%) with PgSPT.

Expression and purification of recombinant P. gingivalis SPT

Recombinant PgSPT was prepared in a manner similar to that described for *S. paucimobilis* SPT (SpSPT;(Raman et al. 2009; Yard et al. 2007)). Briefly, the PgSPT gene (PG1780 from strain W83) was cloned and expressed in *E. coli* from plasmid pET-28a/PgSPT with a 6His-affinity tag at the C-terminus. A combined HisTrap column and size-exclusive chromatography (GE Heatlhcare Sephadex HR S200) approach was used to isolate the dimeric, PLP-bound, holo-form

of the enzyme, and 10% glycerol was added to avoid PgSPT precipitation. The purity of the protein was assessed by SDS-PAGE (Supplemental Figure 1B).

Spectroscopic properties of C' terminal-tagged PgSPT

The UV-visible spectrum of a PLP-dependent enzyme such as SPT usually shows two absorption maxima at 335 nm and 425 nm, due to the properties of the two forms of the internal aldimine PLP Schiff base – enolimine and ketoenamine. In contrast to the SpSPT enzyme, the UV-visible spectrum of PgSPT displays an absorbance maximum at 425 nm suggesting that the PLP cofactor was present predominantly as the ketoenamine form (Figure 1A). By analyzing the change in the absorbance at 425 nm with varying changes in the concentration of L-serine, the dissociation constant (K_d^{Ser}) was determined to be 5.46 ± 0.60 mM (Figure 1B). This value is approximately 5 times weaker than was determined for SpSPT (K_d^{Ser} = 1.1 mM) (Raman et al, 2009).

C' terminal PgSPT activity and kinetics

In order to find the optimal conditions for PgSPT activity, the enzyme was initially tested in buffers of different pH and the highest reaction rate was observed in 100 mM HEPES at pH 7.0. Here we used a convenient coupled assay which uses 5, 5'-dithiobis-2-nitrobenzoic acid (DTNB) reagent which reacts with the CoASH product. The resulting TNB thiolate anion absorbs strongly at 412 nm (ε_{max} = 14,150 M^{-1}, cm^{-1}) (Raman et al. 2009). The enzyme was analyzed with both substrates, L-serine and palmitoyl-CoA to obtain the kinetic parameters, and Michaelis-Menten plot for C' terminal his-tagged PgSPT (Figure 1C and 1D) showed that the

enzyme bound L-serine and palmitoyl-CoA with K_m values of 0.52 ± 0.06 mM and 84 ± 11.7 μM , respectively. The enzyme turned over with a k_{cat} of 43.5 ± 0.4 x 10^{-3} s^{-1} and an efficiency (k_{cat}/K_m) for L-Ser = 84.6 $M^{-1}s^{-1}$ and 524 $M^{-1}s^{-1}$ for pimeloyl-CoA. This compares to similar values determined for SpSPT with respect to substrate binding but with the PgSPT turning over much slower.

Identification of KDS Formation by PgSPT

Since the kinetic assay is indirect and only measures CoASH release, we confirmed that PgSPT catalysed conversion of L-serine and palmitoyl-CoA to the product KDS. For this we used MALDI-TOF MS analysis of the PgSPT assay to detect the formation of the molecular ion related to the product C18:0 KDS [$C_{18}H_{37}NO_2$, M+H]$^+$ (*m/z* 300.290) (Figure 2A). A series of controls (Figure 2B-D) confirmed the KDS was only formed in the presence of the enzyme and both substrates.

RNA-Seq analysis.

The rigid structural characteristic of SLs serves an important functional role in eukaryotic cells by condensing around signaling proteins in the cell membrane and forming densely packed regions of the membrane known as lipid rafts. These puncta of closely-associated lipids and proteins are thought to increase the efficiency of cellular signaling pathways by bringing signaling proteins into close proximity. This information led us to hypothesize that a sphingolipid null mutant may possess a defect in gene expression. Transcriptomic analysis of the SL-null strain in comparison with the parent strain identified 120 genes that were differentially

expressed (≥2-fold, q-value <0.01). Of the 120 genes, the expression of 61 genes were lower; while expression of 59 genes was higher in the SL-null strain. Most notably, three extracytoplasmic function (ECF) sigma factors were found to be differentially expressed: one gene (PG0985) was 3.2-fold lower while the other two (PG0162 and PG0214) were expressed at 2.2-fold and 6.1-fold higher, respectively. In addition, the data show that all of the genes harbored in two distinct loci encoding CRISPR-associated genes (PG1981-PG1989 and PG2013-PG2020) were lower; while genes encoding type IX secretion structural and cargo proteins were among the most over-expressed. As expected, numerous genes encoding hypothetical proteins were differentially expressed (23 reduced and 21 over expressed; Tables 1A and 1B).

Synthesis of SLs by P. gingivalis limits the host capacity to mount a robust pro-inflammatory response.

To examine the contribution of SL-synthesis to the host inflammatory response, we cultured macrophage-like THP-1 cells with *P. gingivalis* wild-type (WT) and the corresponding SPT mutant for up to 24 hours and measured cytokine and chemokine levels. THP-1 is a transformed cell line of human origin. It is a frequently used model cell for investigating macrophage function, a cell that is central to periodontal disease. Our data show that THP-1 cells cultured with the SPT mutant produced a robust immune response which was not observed from cells cultured with the WT (Figure 3). Even as rapidly as 2h after initiation of co-culture, significant increases in the levels of TNF-α, IL-1β, and IL-10 were measured from the cultures infected with the SL-null mutant compared with levels elicited by parent W83 ($p<0.05$ for all by T-test). By 6h, the signature of elevated inflammation initiated by the SPT mutant accelerated, with the addition of a significant increase in IL-6 and RANTES also observed (Figure 3). The

trend of lower cytokine and chemokine production in response to the WT remained evident at 24h of co-culture but trended lower than observed at 6h. No significant differences in THP-1 cell viability was observed between cells cultured with SPT mutant or wild type using MTT assay ($p>0.05$ by ANOVA; Supplemental Table 2). These findings support our hypothesis that in the context of live bacteria, synthesis of SLs limits and/or suppresses the host capacity to mount a robust pro-inflammatory response to this organism.

Transfer of SLs from P. gingivalis to THP-1 cells in a transwell system.

Lastly, we assessed whether SLs could be transferred from *P. gingivalis* to THP-1 macrophages. Employing a 0.4 μm pore transwell system, metabolically-labeled *P. gingivalis* (grown in the presence of PAA, to allow for specific click labeling of SLs with a fluorophore) were placed in the upper-well of the transwell, with THP-1 cells placed in the lower well. After 24h of transwell co-culture, click chemistry verified that *P. gingivalis* SLs were transferred to THP-1 cells without physical contact (Figure 4).

Discussion

P. gingivalis can be present in subgingival plaque even during periodontal health (Griffen et al. 1998), suggesting that the host does not always respond to this bacterium as a pathogen. While other members of the phylum Bacteroidetes, in particular members of the genus *Bacteroides* are viewed as symbiotic or pathobionts, this framework of a symbiotic relationship with the host is not typically applied to *P. gingivalis*. Our view of *P. gingivalis* as a pathobiont (Cugini et al. 2013), led us to consider its unusual ability to synthesize lipids almost identical to its host as a strategy to evade host immune activation.

To evaluate function, gene PG1780, encoding a predicted SPT was cloned and the recombinant protein was isolated, characterized and confirmed as an SPT (PgSPT) by determining the kinetics of the reaction using the canonical substrates L-serine and palmitoyl-CoA. Formation of the KDS product was confirmed by MALDI-TOF-MS analysis. This allowed a comparison with another well characterized bacterial SpSPT from *S. paucimobilis* (Harrison et al. 2019). The PgSPT bound both substrates with a similar affinity to SpSPT but in contrast to this isoform PgSPT displayed much slower kinetics. The molecular details of these differences may be revealed by a comparative x-ray structural analysis and, to that end, crystal trials of PgSPT enzyme is underway. Once the protein structure is known, a comparative evolutionary study of the microbial SPTs will be carried out to explore the species-specific features of the bacterial and eukaryotic SPTs (Harrison et al. 2018; Heaver et al. 2018).

Lipid microdomains are known to position proteins associated with signal transduction, membrane trafficking (protein secretion systems) and regulation of metabolism (protease complexes) in close proximity (Bramkamp and Lopez 2015; Lopez 2015). Given their known function in protein secretion systems, it is tempting to speculate that a subset of the SLs may support T9SS machinery. Furthermore, our RNA-Seq analysis indicates that SLs may indeed stabilize certain proteins involved in signal transduction, in particular sequestration of anti-sigma factors. Anti-sigma factors are known to be localized to the inner membrane where they bind their target ECF sigma factors preventing transcription. Our working model is when SLs are not produced, the targets are over expressed, because the ECF sigma factors are free to interact with target promoters. Some T9SS genes have been shown to be regulated via ECF sigma factors, and we identified fourteen T9SS genes that are expressed at higher levels in the SPT mutant, some as much as 20-fold. Importantly, the genes encoding gingipains were not differentially

279 expressed in the mutant. Our prior studies showed that the SL-null mutant actually demonstrated
280 elevated secreted gingipain activity, not less, suggesting that the higher levels of cytokines is not
281 due to a lack of gingipain activity. That being said, since these proteases are proficient at
282 degrading cytokines, studies are on-going to further evaluate a link between SL synthesis and
283 secreted gingipain activity.

284 Our cell infection modeling shows that SL synthesis leads to a reduced inflammatory
285 response, suggesting that synthesis supports homeostasis. This discovery in some ways
286 contradicts published results. Prior studies using purified *P. gingivalis* SLs point to TLR-2
287 inducing activity (Nichols et al. 2009), stimulation of cellular inflammatory responses (Nichols
288 et al. 2001), and driving of apoptosis (Zahlten et al. 2007). Yet, our findings parallel studies on
289 SL function in other members of the Bacteroidetes that strongly support a role for SLs in
290 immune suppression (An et al. 2011; An et al. 2014; Brown et al. 2019; Heaver et al. 2018).
291 Specifically, a study focused on inflammatory bowel disease (IBD) reported that there is an
292 inverse relationship between SL synthesis by *Bacteroides* and IBD, indicating that bacterial SLs
293 can serve as key factors that mechanistically promote intestinal homeostasis (Brown et al. 2019).
294 As gingival tissues from periodontally healthy and diseased individuals contain SLs, yet the SL
295 types are distinct; our working model has been that SL synthesis not only plays a central role in
296 membrane trafficking in *P. gingivalis*, the secreted SLs may also directly influence host cell
297 function. Our *in vitro* findings agree with clinical findings that *P. gingivalis* releases and/or
298 secrets its SLs; moreover, our findings support that *P. gingivalis* SLs are transferred to host
299 cells. This later discovery is particularly compelling as transfer of SLs from bacteria to host
300 suggests an intriguing interplay, which may serve an important role by which host and microbe
301 interact which in turn, may control oral inflammation as has been shown for *B.*

thetaiotamicron in the gut (Johnson et al. 2019). Lastly, our results show that the absence of SLs elicited high levels of pro- inflammatory cytokines, as well as IL-10, a highly expressed anti-inflammatory cytokine. Our findings of the presence of both pro- and anti-inflammatory cytokines occurring concurrently is not fully understood; however, these results are consistent with clinical profiles observed in inflamed periodontal tissues. The ultimate outcome of this unusual inflammatory pattern requires further evaluation.

In summary, *P. gingivalis* is often described as a master manipulator of the immune response (Hajishengallis and Lamont 2014), primarily due to its ability to degrade immunoglobulins, complement, and cytokines via its repertoire of secreted proteases (Hajishengallis and Lambris 2012). We posit that SL-synthesis is another mechanism of control. Future studies testing these findings in the context of periodontal disease may identify novel approaches to control SL production by *P. gingivalis* and thus shift the balance of inflammation elicited by the subgingival biofilm to a more homeostatic state.

Author contribution

FGR, ZDM, GO, FCG and MED contributed to conception, design, data analysis, and interpretation, drafted and critically revised the manuscript; DC and PT designed, analyzed, and interpreted data regarding PgSPT characterization and critically revised the manuscript. All authors gave final approval and agree to be accountable for all aspects of the work.

The research was supported by the National Institute of Craniofacial Research: R01DE019117 and R01DE24580 (MED) T90 DE021990 (ZDM and FGR) and R90 DE22530 (FGR); as well as start-up funds (FCG and MED)

A supplemental appendix to this article with Materials and Methods and Results is available online.

Acknowledgement

The authors thank the School of Chemistry, University of Edinburgh, and the Edinburgh Global Research Scholarship for PhD studentship funding (PT). The authors would also like to thank Dr. Peter Harrison, Dr. Bohdan Mykhaylyk, Dr. Jo Simpson, Dr. Van Kelly for helpful discussion on SPT, as well as all members of the Davey lab for many helpful discussions on SLs.

We declare that there are no competing financial interests, no conflict of interest.

Figure legends

Figure 1. Characterization of recombinant *P. gingivalis* SPT. (**A**) Absorption UV-visible spectrum of PLP-dependent P. gingivalis SPT. Upon addition of L-serine the enzyme (20 μM) converts from the internal aldimine to the external aldimine form, performed in 20 mM potassium phosphate, 250 mM NaCl, pH 7.5, at 25°C. Solid line (0 mM L-serine), or dashed lines in the presence of 0.1 -100 mM L-serine. (**B**) Analysis of L-serine binding to C-terminal PgSPT by monitoring the change in absorbance at 425 nm. (**C**) Michaelis-Menten kinetic analysis of SPT with substrates L-serine (0.1-100 mM) and palmitoyl-CoA (250 μM) with 1 μM enzyme, 100 mM HEPES, pH 7.0, 250 mM NaCl and 0.2 mM DTNB and measured spectrophotometrically at 412 nm. (**D**) The concentration of L-serine (20 mM) with different palmitoyl-CoA concentrations (1-1000 μM). All data are plotted as mean readings ± 2SD error bars.

Figure 2. MALDI-ToF mass spectra analysis of the PgSPT reaction between L-serine and palmitoyl-CoA. Each assay contained with 1 μM enzyme, 100 mM HEPES, pH 7.0, 250 mM NaCl, 0.2 mM DTNB and 20 mM L-serine or 250 μM palmitoyl-CoA was added dependent on samples. All reaction samples were eluted with 100 % ACN by C4 zip-tip and mixed with CHCA matrix dissolved in 50% ACN within 0.25% TFA. The spectrum was analysed on positive ion mode in triplicates. (**A**) Observation of the product KDS with m/z = 300.290 during a sweep of masses (m/z = 100-800 amu). (**B-D**) Negative controls. (**E**) Full assay with PgSPT, L-serine and P-CoA with a mass range of m/z = 292-304). (**F**) Theoretical mass spectrum based on the KDS formula (M+H)+.

Figure 3. The inability of *P. gingivalis* to synthesize SLs leads to an enhanced cytokine and chemokine response. PMA-treated human macrophage-like THP-1 cells were directly cultured with *P. gingivalis* W83 (WT; gray bars) or the *P. gingivalis* W83 SL-null mutant (SPT; black bars) at MOI 100. Cell culture supernatant fluids were collected at 2, 6 and 24h of co-culture, and the levels of TNFα, IL-1β, IL-6, IL-10, RANTES, and IL-8 were measured by multiplex immunoassay. Medium alone (M; white bars) served as unchallenged control. Data are presented as mean +/- SEM (n = 8 independent experiments); * = $P < 0.05$, and ** = $P < 0.01$ vs. WT *P. gingivalis* using unpaired t-tests.

Figure 4. SLs transfer from *P. gingivalis* to THP-1 cells in a transwell system. (**A**) Epifluorescent image of wild-type W83 bacterial cells showing detection of palmitic acid alkyne (PAA) when bacteria were grown with addition of PAA (green–azide Fluor 488) by click-chemistry. (**B**) As expected, the SPT-null mutant did not incorporate PAA. (**C**) Bright field image of THP-1 cells on cover slip in the lower well of a transwell system after 24hr co-culture with strain W83 (**D**) Epifluorescent image of same THP-1 cells showing DAPI (blue) staining of nucleus, and (**E**) THP-1 cells incorporated the the *P. gingivalis* alkyne tagged SLs (green) that were transferred from W83 constrained to the upper well of the transwell system. (**F**) Click-labeling of THP-1 cells co-cultured with W83 grown in medium without PAA using the transwell system, no green–azide Fluor 488 detected.

Table 1A. Genes expressed at lower levels in the SPT mutant when compared to the parent strain W83.

Name	Gene ID	Product	q-value	Fold Change
SPT	PG1780	serine palmitolytransferase	0	0.01
Proteolysis and amino acid metabolism				
pepD-2	PG0537	aminoacyl-histidine dipeptidase	1.30E-216	0.17
pruA	PG1269	delta-1-pyrroline-5-carboxylate dehydrogenase	2.01E-35	0.38
-	PG1270	PLP-dependent aminotransferase	3.38E-35	0.37
-	PG1271	acetylornithine aminotransferase	2.92E-13	0.38
Transposon				
-	PG0549	ISPg1, transposase	4.72E-19	0.45
-	PG0872	mobilizable transposon, Xis protein	1.20E-09	0.50
-	PG1480	conjugative transposon protein TraI	1.68E-07	0.50
-	PG1482	conjugative transposon protein TraF	1.62E-13	0.33
-	PG1483	conjugative transposon protein TraE	6.11E-11	0.50
Hypothetical				
-	PG0354	hypothetical protein	1.26E-07	0.50
-	PG0554	hypothetical protein	7.25E-13	0.46
-	PG0609	hypothetical protein	6.13E-15	0.50
-	PG0617	hypothetical protein	7.14E-14	0.41
-	PG0727	hypothetical protein	7.89E-57	0.28
-	PG0835	hypothetical protein	2.58E-26	0.33
-	PG0914	hypothetical protein	1.54E-29	0.40
-	PG0986	hypothetical protein	4.38E-24	0.37
-	PG0987	hypothetical protein	1.42E-125	0.21
-	PG1229	hypothetical protein	1.68E-09	0.50
-	PG1268	hypothetical protein	1.54E-53	0.32
-	PG1494	hypothetical protein	5.30E-05	0.50
-	PG1508	hypothetical protein	0.003359	0.35
-	PG1510	hypothetical protein	1.57E-21	0.40
-	PG1511	hypothetical protein	2.39E-21	0.37
-	PG1512	hypothetical protein	2.21E-18	0.36
-	PG1516	hypothetical protein	2.53E-06	0.48
-	PG1547	hypothetical protein	7.02E-06	0.50
-	PG1549	hypothetical protein	4.25E-17	0.33
-	PG1795	hypothetical protein	0.005	0.38
-	PG1798	hypothetical protein	1.79E-12	0.44
-	PG1871	hypothetical protein	7.38E-05	0.33
-	PG1908	hypothetical protein	2.23E-04	0.44
CRISPR loci				
cas2-1	PG1981	CRISPR-associated Cas2 family protein	2.67E-11	0.42
-	PG1982	CRISPR-associated Cas1 family protein	2.27E-12	0.44

-	PG1983	CRISPR-associated Cmr5 family protein	2.25E-06	0.50
-	PG1984	hypothetical protein	1.27E-19	0.33
-	PG1985	CRISPR-associated Cmr4 family protein	1.13E-20	0.42
-	PG1986	CRISPR-associated Cmr3 family protein	2.10E-32	0.35
-	PG1987	CRISPR-associated Csm1 family protein	4.80E-30	0.29
-	PG1988	hypothetical protein	2.31E-40	0.24
-	PG1989	hypothetical protein	6.29E-65	0.27
cas2-2	PG2013	CRISPR-associated Cas2 family protein	2.73E-12	0.47
cas1	PG2014	CRISPR-associated Cas1 family protein	5.31E-31	0.39
cas4	PG2015	CRISPR-associated Cas4 family protein	1.92E-26	0.40
cas3	PG2016	CRISPR-associated helicase Cas3	5.50E-09	0.33
-	PG2017	hypothetical protein	4.44E-14	0.33
-	PG2018	hypothetical protein	3.10E-11	0.33
-	PG2019	hypothetical protein	6.56E-22	0.31
	PG2020	CRISPR-associated Cas5e family protein	?	0.39
Redox homeostasis				
-	PG0616	Thioredoxin	0.003	0.38
Cell wall				
-	PG0726	putative lipoprotein, s-layer	8.42E-08	0.25
Transcription				
-	PG0985	ECF subfamily RNA polymerase sigma factor	3.41E-68	0.29
-	PG1535	transcriptional regulator	1.88E-10	0.50
Metabolism				
hprA	PG1190	glycerate dehydrogenase	8.69E-12	0.49
-	PG1504	NAD dependent protein	0.009	0.33
-	PG1509	HAD superfamily hydrolase	3.63E-24	0.34
-	PG1514	glycerol dehydrogenase	3.16E-11	0.44
-	PG1515	ribulose bisphosphate carboxylase-like protein	1.01E-14	0.45
Biosynthesis of cofactors				
-	PG1505	radical SAM domain-containing protein	3.28E-15	0.32

386 **Table 1B. Genes expressed at higher levels in the SPT mutant when compared to the**
387 **parent strain W83.**
388

Name	Gene ID	Product	q-value	Fold change
Type IX Secretion System				
-	PG0027	hypothetical protein	1.81E-28	2.83
porP	PG0287	hypothetical protein porP	3.33E-56	2.58
porK	PG0288	putative lipoprotein porK	1.24E-32	2.65
porL	PG0289	hypothetical protein porL	1.14E-40	2.56
porM	PG0290	hypothetical protein porM	8.78E-20	2.21
porN	PG0291	hypothetical protein porN	2.53E-29	2.58
porT	PG0751	porT protein	8.54E-30	2.00
sov	PG0809	hypothetical protein	3.61E-10	2.10
	PG0810	hypothetical protein	4.20E-55	2.60
tpr	PG1055	thiol protease	0	8.00
-	PG1947	hypothetical protein	1.48E-17	2.00
TapA	PG2100	TapA	0	10.88
TapB	PG2101	TapB	0	20.33
TapC	PG2102	TapC	0	20.33
Hypothetical and other				
ispF	PG0028	2-C-methyl-D-erythritol 2,4-cyclodiphosphate synthase	1.19E-28	2.20
-	PG0161	hypothetical protein	1.58E-134	3.34
-	PG0216	hypothetical protein	1.49E-182	4.80
-	PG0217	hypothetical protein	1.57E-298	4.69
-	PG0218	hypothetical protein	0	5.00
-	PG0241	putative lipoprotein	2.60E-05	2.07
-	PG0297	hypothetical protein	1.52E-18	2.00
-	PG0323	hypothetical protein	2.96E-36	2.31
-	PG0419	hypothetical protein	7.47E-20	2.27
-	PG0606	hypothetical protein	2.13E-29	2.25
-	PG0607	hypothetical protein	3.11E-13	2.44
clpB	PG1118	clpB protein	9.12E-23	2.28
-	PG1374	hypothetical protein	6.87E-16	2.51
-	PG1527	hypothetical protein	1.39E-19	2.00
-	PG1571	metallo-beta-lactamase superfamily protein	5.44E-10	2.00
-	PG1625	hypothetical protein	1.62E-11	2.17
-	PG1626	hypothetical protein	3.75E-17	2.32
-	PG1634	hypothetical protein	3.84E-20	2.16
-	PG1662	hypothetical protein	7.73E-27	2.12
-	PG1682	glycosyl transferase	8.04E-54	2.44
-	PG1683	hypothetical protein	2.03E-26	2.10
-	PG1684	hypothetical protein	5.65E-42	3.20
udk	PG1781	uridine kinase	2.11E-30	2.30

-	PG1835	putative lipoprotein	3.05E-10	2.12
aroA	PG1944	3-phosphoshikimate 1-carboxyvinyltransferase	1.40E-20	2.04
-	PG1945	hypothetical protein	3.76E-34	2.31
-	PG1967	hypothetical protein	2.07E-34	2.33
-	PG2103	hypothetical protein	1.68E-37	2.30
Transport				
-	PG0064	CzcA family heavy metal efflux protein	3.76E-42	2.29
-	PG0280	ABC transporter permease	1.97E-11	2.00
-	PG0281	ABC transporter permease	2.05E-14	2.00
-	PG0282	ABC transporter ATP-binding protein	4.46E-13	3.00
-	PG0680	RND family efflux transporter MFP subunit	3.77E-07	2.00
-	PG1010	ABC transporter ATP-binding protein	5.74E-33	2.00
-	PG1117	MATE efflux family protein	1.10E-07	2.00
-	PG1176	ABC transporter ATP-binding protein	0.001661967	2.00
-	PG1663	ABC transporter ATP-binding protein	6.34E-34	2.05
-	PG1664	ABC transporter permease	2.07E-33	2.11
-	PG1665	ABC transporter permease	3.06E-24	2.00
-	PG1946	ABC transporter	1.56E-25	2.25
Transcription				
-	PG0162	ECF subfamily RNA polymerase sigma factor	4.84E-10	2.10
-	PG0214	ECF subfamily RNA polymerase sigma factor	0	5.87
-	PG0215	Putative anti-sigma factor	1.25E-199	4.46
-	PG1007	GntR family transcriptional regulator	9.11E-24	2.10

389
390

References

An D, Na C, Bielawski J, Hannun YA, Kasper DL. 2011. Membrane sphingolipids as essential molecular signals for *Bacteroides* survival in the intestine. Proceedings of the National Academy of Sciences of the United States of America. 108 Suppl 1:4666-4671.

An D, Oh SF, Olszak T, Neves JF, Avci FY, Erturk-Hasdemir D, Lu X, Zeissig S, Blumberg RS, Kasper DL. 2014. Sphingolipids from a symbiotic microbe regulate homeostasis of host intestinal natural killer t cells. Cell. 156(1-2):123-133.

Bramkamp M, Lopez D. 2015. Exploring the existence of lipid rafts in bacteria. Microbiol Mol Biol Rev. 79(1):81-100.

Brown EM, Ke X, Hitchcock D, Jeanfavre S, Avila-Pacheco J, Nakata T, Arthur TD, Fornelos N, Heim C, Franzosa EA et al. 2019. Bacteroides-derived sphingolipids are critical for maintaining intestinal homeostasis and symbiosis. Cell Host Microbe. 25(5):668-680 e667.

Byrne SJ, Dashper SG, Darby IB, Adams GG, Hoffmann B, Reynolds EC. 2009. Progression of chronic periodontitis can be predicted by the levels of *Porphyromonas gingivalis* and treponema denticola in subgingival plaque. Oral Microbiol Immunol. 24(6):469-477.

Cugini C, Klepac-Ceraj V, Rackaityte E, Riggs JE, Davey ME. 2013. *Porphyromonas gingivalis:* Keeping the pathos out of the biont. Journal of oral microbiology. 5.

Darveau RP. 2010. Periodontitis: A polymicrobial disruption of host homeostasis. Nat Rev Microbiol. 8(7):481-490.

Dunn TM, Tifft CJ, Proia RL. 2019. A perilous path: The inborn errors of sphingolipid metabolism. J Lipid Res. 60(3):475-483.

Griffen AL, Becker MR, Lyons SR, Moeschberger ML, Leys EJ. 1998. Prevalence of *Porphyromonas gingivalis* and periodontal health status. J Clin Microbiol. 36(11):3239-3242.

Hajishengallis G, Lambris JD. 2012. Complement and dysbiosis in periodontal disease. Immunobiology. 217(11):1111-1116.

Hajishengallis G, Lamont RJ. 2014. Breaking bad: Manipulation of the host response by *Porphyromonas gingivalis*. Eur J Immunol. 44(2):328-338.

Hannun YA, Obeid LM. 2008. Principles of bioactive lipid signalling: Lessons from sphingolipids. Nat Rev Mol Cell Biol. 9(2):139-150.

Hannun YA, Obeid LM. 2018. Sphingolipids and their metabolism in physiology and disease. Nature reviews. 19(3):175-191.

Harrison PJ, Dunn TM, Campopiano DJ. 2018. Sphingolipid biosynthesis in man and microbes. Nat Prod Rep. 35(9):921-954.

Harrison PJ, Gable K, Somashekarappa N, Kelly V, Clarke DJ, Naismith JH, Dunn TM, Campopiano DJ. 2019. Use of isotopically labeled substrates reveals kinetic differences between human and bacterial serine palmitoyltransferase (vol 60, pg 953, 2019). Journal of Lipid Research. 60(8):1489-1489.

Heaver SL, Johnson EL, Ley RE. 2018. Sphingolipids in host-microbial interactions. Current opinion in microbiology. 43:92-99.

Johnson EL, Heaver SL, Waters JL, Kim BI, Bretin A, Goodman AL, Gewirtz AT, Worgall TS, Ley RE. 2019. Sphingolipid production by gut Bacteroidetes regulates glucose homeostasis. bioRxiv.

435 Kanzaki H, Movila A, Kayal R, Napimoga MH, Egashira K, Dewhirst F, Sasaki H, Howait M,
436 Al-Dharrab A, Mira A et al. 2017. Phosphoglycerol dihydroceramide, a distinctive
437 ceramide produced by *Porphyromonas gingivalis*, promotes rankl-induced
438 osteoclastogenesis by acting on non-muscle myosin ii-a (myh9), an osteoclast cell fusion
439 regulatory factor. Biochim Biophys Acta Mol Cell Biol Lipids. 1862(5):452-462.
440 Lamont RJ, Jenkinson HF. 1998. Life below the gum line: Pathogenic mechanisms of
441 *Porphyromonas gingivalis*. Microbiol Mol Biol Rev. 62(4):1244-1263.
442 Lopez D. 2015. Molecular composition of functional microdomains in bacterial membranes.
443 Chem Phys Lipids. 192:3-11.
444 Maceyka M, Spiegel S. 2014. Sphingolipid metabolites in inflammatory disease. Nature.
445 510(7503):58-67.
446 Merrill AH, Jr., Carman GM. 2015. Introduction to thematic minireview series: Novel bioactive
447 sphingolipids. J Biol Chem. 290(25):15362-15364.
448 Moradali MF, Ghods S, Angelini TE, Davey ME. 2019. Amino acids as wetting agents: Surface
449 translocation by Porphyromonas gingivalis. ISME J 13(6): 1560-1574.
450 Moye ZD, Gormley CM, Davey ME. 2019. Galactose impacts the size and intracellular
451 composition of the asaccharolytic oral pathobiont *Porphyromonas gingivalis*. Appl
452 Environ Microbiol 85(4).
453 Moye ZD, Valiuskyte K, Dewhirst FE, Nichols FC, Davey ME. 2016. Synthesis of sphingolipids
454 impacts survival of *Porphyromonas gingivalis* and the presentation of surface
455 polysaccharides. Front Microbiol. 7:1919.
456 Nichols FC. 1998. Novel ceramides recovered from *Porphyromonas gingivalis*: Relationship to
457 adult periodontitis. J Lipid Res. 39(12):2360-2372.
458 Nichols FC, Housley WJ, O'Conor CA, Manning T, Wu S, Clark RB. 2009. Unique lipids from a
459 common human bacterium represent a new class of toll-like receptor 2 ligands capable of
460 enhancing autoimmunity. Am J Pathol. 175(6):2430-2438.
461 Nichols FC, Levinbook H, Shnaydman M, Goldschmidt J. 2001. Prostaglandin e2 secretion from
462 gingival fibroblasts treated with interleukin-1beta: Effects of lipid extracts from
463 *Porphyromonas gingivalis* or calculus. J Periodontal Res. 36(3):142-152.
464 Nichols FC, Riep B, Mun J, Morton MD, Bojarski MT, Dewhirst FE, Smith MB. 2004.
465 Structures and biological activity of phosphorylated dihydroceramides of *Porphyromonas*
466 *gingivalis*. J Lipid Res. 45(12):2317-2330.
467 Nichols FC, Rojanasomsith K. 2006. *Porphyromonas gingivalis* lipids and diseased dental
468 tissues. Oral Microbiol Immunol. 21(2):84-92.
469 Nichols FC, Yao X, Bajrami B, Downes J, Finegold SM, Knee E, Gallagher JJ, Housley WJ,
470 Clark RB. 2011. Phosphorylated dihydroceramides from common human bacteria are
471 recovered in human tissues. PLoS One. 6(2):e16771.
472 Olsen I, Jantzen E. 2001. Sphingolipids in bacteria and fungi. Anaerobe. 7(2):103-112.
473 Olsen I, Nichols FC. 2018. Are sphingolipids and serine dipeptide lipids underestimated
474 virulence factors of porphyromonas gingivalis? Infect Immun. 86(7).
475 Raman MC, Johnson KA, Yard BA, Lowther J, Carter LG, Naismith JH, Campopiano DJ. 2009.
476 The external aldimine form of serine palmitoyltransferase: Structural, kinetic, and
477 spectroscopic analysis of the wild-type enzyme and hsan1 mutant mimics. J Biol Chem.
478 284(25):17328-17339.
479 Socransky SS, Haffajee AD, Cugini MA, Smith C, Kent RL, Jr. 1998. Microbial complexes in
480 subgingival plaque. J Clin Periodontol. 25(2):134-144.

Vermilyea DM, Ottenberg GK, Davey ME. 2019. Citrullination mediated by PPAD constrains biofilm formation in *P. gingivalis* strain 381. NPJ Biofilms Microbiomes. 5:7.

Yard BA, Carter LG, Johnson KA, Overton IM, Dorward M, Liu H, McMahon SA, Oke M, Puech D, Barton GJ et al. 2007. The structure of serine palmitoyltransferase; gateway to sphingolipid biosynthesis. Journal of molecular biology. 370(5):870-886.

Zahlten J, Riep B, Nichols FC, Walter C, Schmeck B, Bernimoulin JP, Hippenstiel S. 2007. *Porphyromonas gingivalis* dihydroceramides induce apoptosis in endothelial cells. J Dent Res. 86(7):635-640.

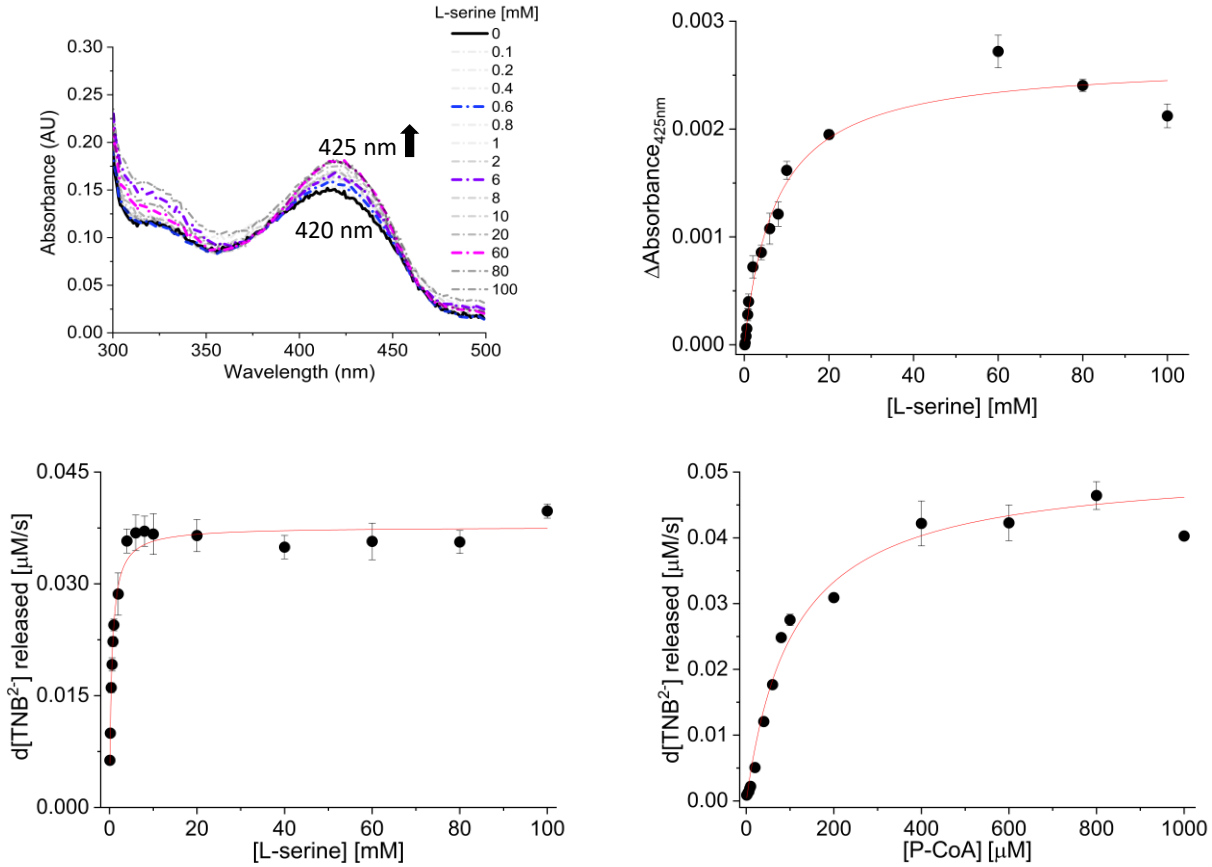

Figure 1. Characterization of recombinant *P. gingivalis* SPT. (A) Absorption characteristics (UV-visible spectrum) of PLP-dependent *P. gingivalis* SPT. Upon addition of L-serine the enzyme (20 μM) converts from the internal aldimine to the external aldimine form, assay performed in 20 mM potassium phosphate, 250 mM NaCl, pH 7.5, at 25 °C. Solid line (0 mM L-serine), or dashed lines in the presence of 0.1 -100 mM L-serine. **(B)** Analysis of L-serine binding to C-terminal PgSPT by monitoring the change in absorbance at 425 nm. **(C)** Michaelis-Menten kinetic analysis of SPT with substrates L-serine (0.1-100 mM) and palmitoyl-CoA (250 μM) with 1 μM enzyme, 100 mM HEPES, pH 7.0, 250 mM NaCl and 0.2 mM DTNB and measured spectrophotometrically at 412 nm. **(D)** The concentration of L-serine (20 mM) with different palmitoyl-CoA concentrations (1-1000 μM). All data are plotted as mean readings ± 2SD error bars.

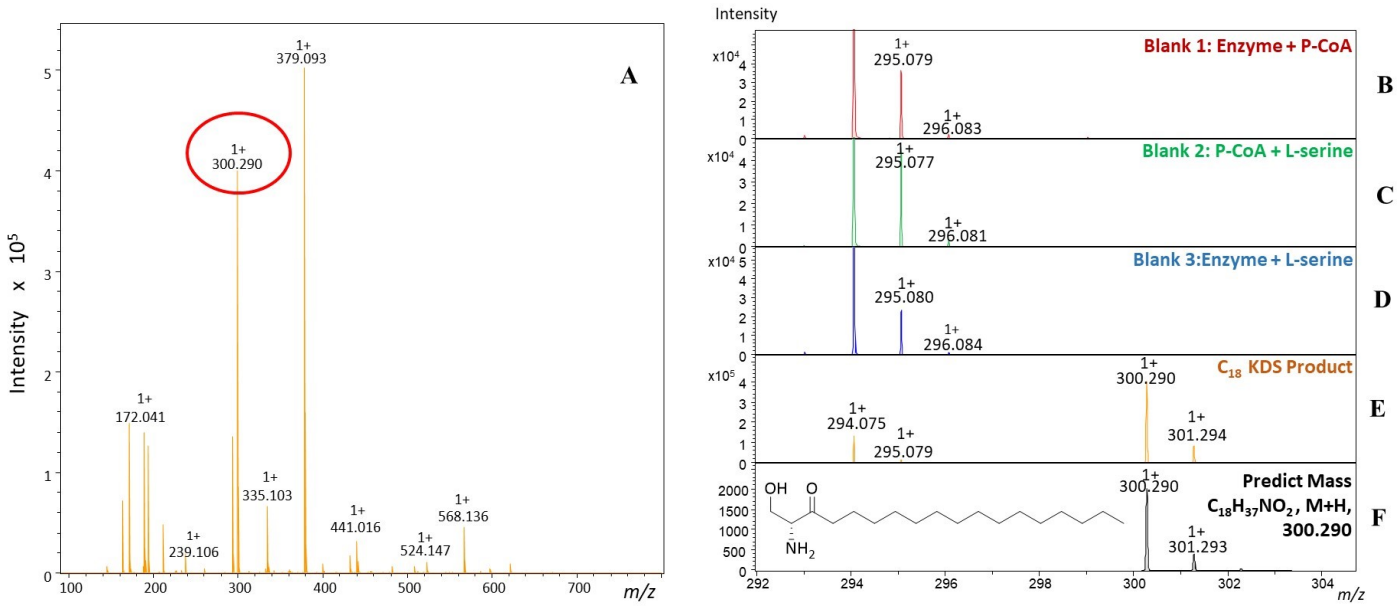

Figure 2. MALDI-ToF mass spectra analysis of the PgSPT reaction between L-serine and palmitoyl-CoA. Each assay contained with 1 µM enzyme, 100 mM HEPES, pH 7.0, 250 mM NaCl, 0.2 mM DTNB and 20 mM L-serine or 250 µM palmitoyl-CoA was added dependent on samples. All reaction samples were eluted with 100 % ACN by C4 zip-tip and mixed with CHCA matrix dissolved in 50% ACN within 0.25% TFA. The spectrum was analysed on positive ion mode in triplicates. **(A)** Observation of the product KDS with *m/z* = 300.290 during a sweep of masses (*m/z* = 100-800 amu). (**B-D**) Negative controls. **(E)** Full assay with PgSPT, L-serine and P-CoA with a mass range of *m/z* = 292-304). (**F**) Theoretical mass spectrum based on the KDS formula $(M+H)^+$.

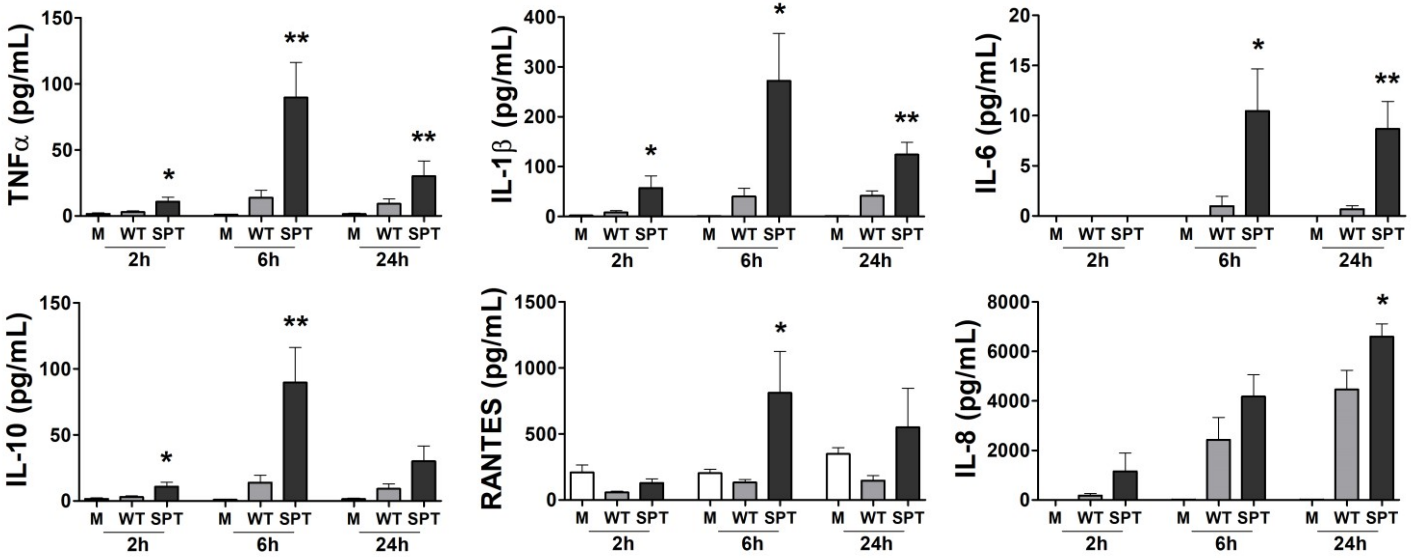

Figure 3. The inability of *P. gingivalis* to synthesize SLs leads to an enhanced cytokine and chemokine response. PMA-treated human macrophage-like THP-1 cells were directly cultured with *P. gingivalis* W83 (WT; gray bars) or the *P. gingivalis* W83 SL-null mutant (SPT; black bars) at MOI 100. Cell culture supernatant fluids were collected at 2, 6 and 24h of co-culture, and the levels of TNFα, IL-1β, IL-6, IL-10, RANTES, and IL-8 were measured by multiplex immunoassay. Medium alone (M; white bars) served as unchallenged control. Data are presented as mean +/- SEM (n = 8 independent experiments); * = P <0.05, and ** = P <0.01 vs. WT *P. gingivalis* using unpaired t-tests.

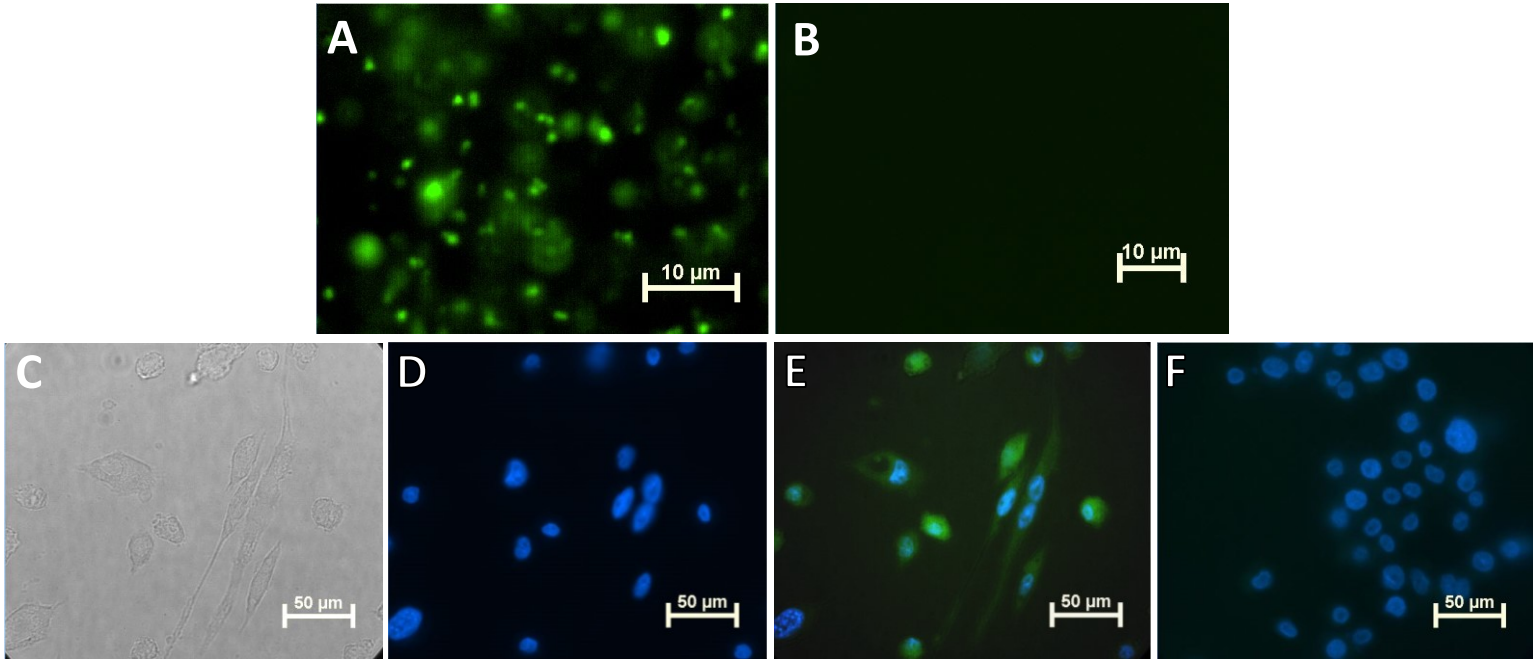

Figure 4. SLs transfer from *P. gingivalis* to THP-1 cells in a transwell system. (**A**) Epifluorescent image of wild-type W83 bacterial cells showing detection of palmitic acid alkyne (PAA) when bacteria were grown with addition of PAA (green–azide Fluor 488) by click-chemistry. (**B**) As expected, the SPT-null mutant did not incorporate PAA. (**C**) Bright field image of THP-1 cells on cover slip in the lower well of a transwell system after 24hr co-culture with strain W83 (**D**) Epifluorescent image of same THP-1 cells showing DAPI (blue) staining of nucleus, and (**E**) THP-1 cells incorporated the the *P. gingivalis* alkyne tagged SLs (green) that were transferred from W83 constrained to the upper well of the transwell system. (**F**) Click-labeling of THP-1 cells co-cultured with W83 grown in medium without PAA using the transwell system, no green–azide Fluor 488 detected.